

Secondary halo bias through cosmic time II: Reconstructing halo properties using clustering information

Andrés Balaguera-Antolínez^{1,2*} and Antonio D. Montero-Dorta³

¹ Instituto de Astrofísica de Canarias, s/n, E-38205, La Laguna, Tenerife, Spain

² Departamento de Astrofísica, Universidad de La Laguna, E-38206, La Laguna, Tenerife, Spain

³ Departamento de Física, Universidad Técnica Federico Santa María, Casilla 110-V, Avda. España 1680, Valparaíso, Chile

Received / Accepted

ABSTRACT

Context. When constructing galaxy mock catalogs based on suites of dark matter halo catalogs generated with approximated, calibrated or machine-learning approaches, the assignment of intrinsic properties for such tracers is a step of paramount relevance, given that these can shape the abundance and spatial distribution of mock galaxies and galaxy clusters.

Aims. We explore the possibility to assign properties of dark matter halos within the context of calibrated/learning approaches, explicitly using clustering information. The goal is to retrieve the correct signal of primary and secondary large-effective bias as a function of properties reconstructed solely based on phase-space properties of the halo distribution and dark matter density field.

Methods. The algorithm reconstructs a set halo properties (such as virial mass, maximum circular velocity, concentration and spin) constraint to reproduce both primary and secondary (or assembly) bias. The key ingredients of the algorithm are the implementation of individually-assigned large-scale effective bias, a multi-scale approach to account for halo exclusion and a hierarchical assignment of halo properties.

Results. The method facilitates the assignment of halo properties aiming at replicating the large-scale effective bias, both primary and secondary. This improves over previous methods in the literature, especially at the high-mass end population.

Conclusions. We have designed an strategy to reconstruct the main properties of dark matter halos obtained by calibrated/learning algorithms, such that the one and two-point statistics (on large scales) replicates the signal from detailed N -body simulations. We encourage the application of this strategy (or the implementation of our algorithm) for the generation of mock catalogs of dark matter halos based on approximated methods.

Key words. Cosmology: large-scale structure of the Universe – Galaxies:

1. Introduction

Mock catalogs of galaxies and galaxy clusters are essential tools for the statistical analysis of galaxy redshift surveys (such as EUCLID (Amendola et al. 2016), DESI (Levi et al. 2013), J-PAS (Benitez et al. 2014), or the *Nancy Grace Roman* space telescope (Spergel et al. 2015)). Their usefulness lies not only in their capability to capture the main statistical properties of the spatial distribution of dark matter tracers in the Universe (n -point statistics), but also the behavior of such properties as a function of a number of intrinsic properties (e.g., luminosity, stellar mass, color, star formation rate) which are key to understand the processes of galaxy cluster assembly and galaxy formation and evolution (see e.g., Euclid Collaboration et al. 2024).

Intrinsic galaxy and galaxy cluster properties in mock catalogs can be robustly derived from high resolution hydro-simulations (e.g., Nelson et al. 2019; Dubois et al. 2021; Feldmann et al. 2023), the cost of which typically scales with the size of the sample aimed at being reproduced, along with the details of the baryonic process involved,

making this path demanding at replicating the vast cosmological volumes currently surveyed. While this obstacle is rapidly being overcome (see e.g. Schaye et al. 2023), the true difficulty arises when thousand of realizations of such type of simulations are needed for covariance matrix analysis. Dark matter only simulations (see e.g., Angulo & Hahn 2022, and references therein) can replicate large cosmological volumes with samples of halos and sub-halos, on top of which galaxies can be placed using a number of techniques, such as the halo occupation distribution techniques (see e.g., Cooray 2002; Cooray & Sheth 2002; Berlind & Weinberg 2002; Kravtsov et al. 2004) or the sub-halo abundance matching (see e.g., Vale & Ostriker 2004; Kravtsov et al. 2004; Conroy et al. 2006; Favole et al. 2016). In this scenario, halo properties are robustly derived from the distribution of dark matter particles (see e.g., Mansfield & Avestruz 2021, and references therein), and used as proxies for the generation of galaxy positions and intrinsic properties. However, dark matter only simulations can be also expensive in terms of computing time, due to the large volumes and the high mass resolution needed to accurately resolve halos and sub-halos containing the type of observed

* balaguera@iac.es

galaxies (for example, luminous red galaxies, emission-line galaxies) and again, the number of realizations demanded for robust estimates of covariance matrices.

Approximated methods (see e.g. Bond & Myers 1996; Scoccimarro & Sheth 2002; Manera et al. 2013; Sousbie et al. 2008; Monaco et al. 2002, 2013; Munari et al. 2017; Berner et al. 2022; Tassev et al. 2013; Koda et al. 2016; Izard et al. 2018; White et al. 2014; Howlett et al. 2015; Feng et al. 2016; Kitaura et al. 2014; Avila et al. 2015; Balaguera-Antolínez et al. 2019; Balaguera-Antolínez et al. 2020, 2023; Baratta et al. 2020, 2022, and references therein) and learning approaches (see e.g., Zhang et al. 2019; He et al. 2019; Villaescusa-Navarro et al. 2021; Piras et al. 2023; Ding et al. 2024) have been shown to provide fast and relatively accurate (on scales of interest) realizations of dark matter halos with phase-space coordinates. Nevertheless, for these methods to be applicable to build galaxy mock catalogs, they need to surmount one difficulty, namely, the accomplishment of a precise assignment of halo intrinsic properties (e.g., virial mass, velocity dispersion, concentration, spin). Such task is key because the abundance and clustering probes of dark matter tracers, when explored as a function of intrinsic properties (e.g. stellar masses, X-ray luminosities) is very sensitive to the underlying scaling relations adopted to assign these properties (see e.g. Balaguera-Antolínez et al. 2012, for an example on the construction of mock catalogs for galaxy clusters). The assignment of halo properties constrained to reproduce the large-scale clustering signal is the scientific target of this paper, which represents the second in a number of papers dedicated to the connection between halo properties and large-scale structure (Balaguera-Antolínez et al. 2024).

Keeping in mind that N -body simulations can be considered to provide, to knowledge, the most realistic representation of the distribution of dark matter halos and its statistical properties in a cosmological volume, the precision of an assignment procedure can be captured in the comparison of a number of statistics, such as the halo abundance, scaling relations among the halo properties, and two (and higher) order statistics, with respect to the corresponding N -body estimates. In particular, the signature of large-scale effective bias (see e.g., Kaiser 1984; Fry & Gaztanaga 1993; Kauffmann et al. 1997; Sheth & Tormen 2004; Gao et al. 2005; Wechsler et al. 2006; Gao & White 2007; Croton et al. 2007; Angulo et al. 2008; Dalal et al. 2008; Faltenbacher & White 2010; Lee et al. 2017; Lazeyras et al. 2017; Montero-Dorta et al. 2017; Mao et al. 2018; Musso et al. 2018; Sato-Polito et al. 2019; Contreras et al. 2019; Montero-Dorta et al. 2020, 2021; Xu et al. 2021; Lee & Moon 2024; Montero-Dorta & Rodriguez 2024) is key to connect models of galaxy/halo population with the measurements of abundance and clustering as a function of a given property. Retrieving this signal with accuracy is particularly difficult in the context of calibrated/learning oriented methods (where only phase-space coordinates are available), and the assignment of properties can only be done through the mining of the correlation between those halo properties and the underlying dark matter density field. Different approaches (e.g., Zhao et al. 2015; Balaguera-Antolínez et al. 2023; Fang et al. 2024) have been proposed to perform this task, using local-and non-local properties on the underlying dark matter density field. Although such information helps to reproduce the clustering signal as a function of halo number counts (see e.g., Balaguera-Antolínez et al. 2019), it is not

sufficient to fully replicate the signal of primary (i.e, clustering as a function of a primary halo property) and secondary large-scale bias (i.e, dependency of halo clustering on a secondary halo property at fixed values of primary property), specially for massive halos (see e.g., Wong & Taylor 2012; Balaguera-Antolínez et al. 2023). It is key to emphasize, in this context, that methods designed to assign galaxy properties to sub-halos based on the properties of parent halos (as e.g. machine learning approaches, see e.g., Ramakrishnan et al. 2021; Forero-Sánchez et al. 2022; de Santi et al. 2022; Rodrigues et al. 2023) can reproduce the large-scale bias, mainly due to the fact that such signature is already encoded in the parent halo properties used to learn from.

In this work we present the multi-scale halo property assignment (MSHA hereafter) algorithm, designed to provide intrinsic properties to dark matter halos through the assessment of the scaling relation between halo properties and the statistical properties of dark matter and dark matter halos. As a novelty, the algorithm uses the assignment of individual large-scale effective halo bias (see e.g., Paranjape et al. 2018), which has provided a novel window for the analysis of primary and secondary halo bias (see e.g., Contreras et al. 2021; Balaguera-Antolínez et al. 2024), along with a multi-scale strategy to account for halo exclusion.

To assess the performance of the strategy proposed in the MSHA, we use the UNITSim¹ (Chuang et al. 2019), which consists in a set of paired-fixed amplitude (Angulo & Pontzen 2016) cosmological N -body simulation, evolved from redshift $z = 99$ until $z = 0$ in a cosmological volume of $1(\text{Gpc}h^{-1})^3$ (see e.g., Angulo & Pontzen 2016; Garrison et al. 2018; Villaescusa-Navarro et al. 2018; Chuang et al. 2019; Zhai et al. 2019; Klypin et al. 2020; Maksimova et al. 2021, for more details in this type of simulations). The dark matter field (constructed from 4096^3 dark matter particles) is represented by a mesh of $N_m^3 = 256^3$, and halo catalogs are built using the ROCKSTAR algorithm (Behroozi et al. 2013), with a minimum halo-mass of $2 \times 10^{11} M_\odot h^{-1}$ (see Balaguera-Antolínez et al. 2024, for more details on the halo properties in this simulation). In forthcoming publications we shall describe ongoing developments on the assignment algorithm as well as applications to light-cones.

The structure of this paper is as follows. In §2 we present the halo and dark matter field properties used in the MSHA algorithm. In §3 we describe its main features and present an example of the performance in §4. We end with discussions in §5, and end with conclusions.

2. Dark matter and dark matter halo properties

2.1. Properties of the dark matter density field

Statistical properties of the dark matter distribution $\delta_{\text{dm}}(\mathbf{r})$, such as the local density or tidal field² are key to reproduce halo number counts with precise two and three-point statistics (see e.g., Balaguera-Antolínez et al. 2019; Pellejero-Ibañez et al. 2020; Balaguera-Antolínez et al. 2020, 2023; Bartlett et al. 2024). The information of the tidal field can be used in the form of a cosmic-web classification (i.e., knots, filaments, sheets, voids; see, e.g., Hahn et al. 2007; van de Weygaert et al. 2009; Forero-Romero et al. 2009;

¹ <http://www.unitsims.org/>

² With components $\mathcal{T}_{ij} = \partial_i \partial_j \phi$, where ϕ satisfies Poisson equation $\nabla^2 \phi = \delta_{\text{dm}}$

Aragon-Calvo 2016; Yang et al. 2017; Paranjape et al. 2018) or through the construction of combinations of its eigenvalues such as its invariants (see e.g., Paranjape et al. 2018; Kitaura et al. 2022), the prolateness, the ellipticity (see e.g., Mo et al. 2010), the tidal anisotropy parameter, (see e.g., Paranjape et al. 2018) or the mass of collapsing regions (see e.g., Zhao et al. 2015; Balaguera-Antolínez et al. 2019). In this work we use the information of the local density and the cosmic-web classification as the main dark matter properties (hereafter $\{\Theta\}_{\text{dm}}$), as input of the MSHA algorithm. The details on these properties, computed for the reference simulation, can be found at Balaguera-Antolínez et al. (2024).

2.2. Environmental halo properties

Following Balaguera-Antolínez et al. (2024), we compute for each tracer a number of properties $\{\Theta\}_{\text{H}}$ by collecting information of the surrounding tracers within a sphere of radius R , namely i) the so-called relative local mach number \mathcal{M}_R and ii) the local overdensity δ_R . The relative local mach number is measure of the local kinematic temperature of the tracer distribution (see e.g., Nagamine et al. 2001; Agarwal & Feldman 2013; Meriot et al. 2022)), while the local overdensity δ_R is defined as the excess of tracers with respect to the mean number density around each tracer. The scale R used in the computation of these quantities is in principle a free parameter. We have chosen $R = 3 \text{ Mpc}/h$, a scale in which both cosmic-web environment and local overdensity help to shape the halo number clustering (see e.g., Wu et al. 2024). The analysis by Balaguera-Antolínez et al. (2024) demonstrated that these environmental properties display the largest correlations with the large-scale effective bias.

2.3. Individual large-scale effective bias

Following Paranjape et al. (2018); Ramakrishnan et al. (2019); Han et al. (2019); Paranjape & Alam (2020); Contreras et al. (2021); Balaguera-Antolínez et al. (2024) we assign an effective large-scale halo bias to each tracer (with position \mathbf{r}_i) as:

$$b_{\text{eff}}^{(i)} = \frac{\sum_{j,k_j < k_{\text{max}}} N_k^j \langle e^{-i\mathbf{k}\cdot\mathbf{r}_i} \delta_{\text{dm}}^*(\mathbf{k}) \rangle_{k_j}}{\sum_{j,k_j < k_{\text{max}}} N_k^j P_{\text{dm}}(k_j)}, \quad (1)$$

where $\delta_{\text{dm}}(\mathbf{k})$ is the Fourier transform of the dark matter density field, $P_{\text{dm}}(k_j)$ its power spectrum and N_k^j is the number of Fourier modes in the j -the spherical bin in Fourier space. The sum is carried over the range of wavenumbers $k_j < k_{\text{max}}$ in which the ratio between the halo and the dark matter power spectra is constant³. Balaguera-Antolínez et al. (2024) showed that the effective bias as a function of multiple halo properties, as obtained from standard approaches (for example, measurements of auto and cross-power halo power spectrum in bins of that halo property, see e.g., Balaguera-Antolínez 2014; Pollack et al. 2014), is consistent with the results obtained from Eq. (1) and with known calibrations in the literature, such as the bias - halo mass relation (Tinker et al. 2010, see also Paranjape et al.

³ We have used a maximum wavenumber $k_{\text{max}} = 0.08 h \text{Mpc}^{-1}$, up to which, at the redshifts explored in this work, the ratio $P_h(k)/P_{\text{dm}}(k)$ is compatible with a constant value.

2018). Assigning a bias to each object allows us to include clustering signal (up to a given scale k_{max}) to the machinery for assigning halo properties. Notice that we can also compute secondary bias (see e.g., Smith et al. 2009), which can help to improve the signal of higher order statistics in terms of halo properties. For the purpose of this work, we only use the effective bias and leave quadratic bias for a forthcoming research.

Compared with previous attempts to assign halo properties, the inclusion of the large-scale effective bias is key to retrieve properties that replicate the large-scale pattern as drawn by such tracers. As we will show in the following sections, not including this bias yields halo properties which, even if depicting the correct abundance, fail, particularly at the high mass end of the halo mass function, at reproducing primary and secondary bias, even if non-local properties of the dark matter field are included.

2.4. Target halo properties

Let us briefly describe the halo properties we will aim at reconstructing. In general, the properties of dark matter halos can be separated in a primary η_p and secondary η_s set. The definition of these sets can be established by a number of ways, such as correlation with the underlying dark matter density field (see e.g., Balaguera-Antolínez et al. 2023) or a principal component analysis of the halo properties (Skibba & Macciò 2011; Zhou et al. 2023; Balaguera-Antolínez et al. 2024). We can call “primary” properties as those directly probing the depth of the potential wells of dark matter halos, such as virial mass, velocity dispersion or maximum circular velocity V_{max} (see e.g., Zehavi et al. 2019). In this work we use the latter as main property, followed by the virial mass M_{vir} . As secondary, we use halo spin (Bullock et al. 2001) and the halo concentration $C_{\text{vir}} \equiv R_{\text{vir}}/R_s$, where R_{vir} is the virial radius and R_s the scale radius, obtained based on fits to a NFW profile (Navarro et al. 1996) within the ROCKSTAR algorithm (see e.g., Knebe et al. 2011; Mansfield & Kravtsov 2020).

3. The algorithm

The MSHA algorithm⁴ aims at assigning halo intrinsic properties (as those discussed in §2.4) constrained to provide the correct large-scale clustering signal as a function of those properties. The input of the algorithm is made up by two components, namely:

- A reference simulation, which is ideally one (or a number of) realization(s) of a tracer distribution in an N -body simulation, from which we can have access to dark matter density field and a halo catalog (with intrinsic properties).
- A target or mock realization of dark matter halos (with phase space coordinates) together with its corresponding dark matter density field.

Two main features characterize this algorithm. On one hand, we explicitly implement the assignment of individual halo bias of Eq. (1) to mine its correlations with halo properties (Balaguera-Antolínez et al. 2024). This is a key ingredient, as it directs the distribution of halo properties

⁴ The MSHA algorithm is part of the C++ library `CosmicCodes` found at <https://github.com/balaguera/CosmicCodes>.

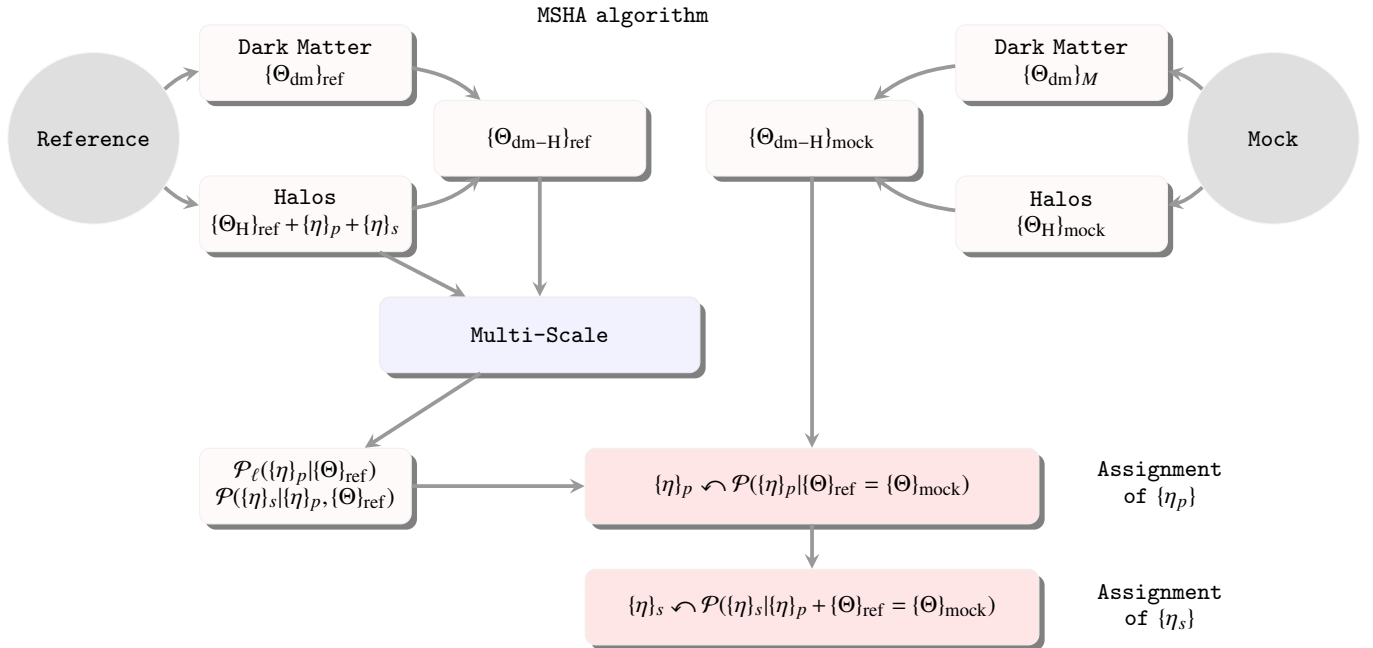


Fig. 1: Flow-chart representing the algorithm designed to assign halo properties. The reference simulation provides a dark matter density field and its corresponding halo catalogs, with phase-space coordinates and intrinsic properties.

towards the correct large-scale signal when the two-point statistics of tracers is assessed as a function of their intrinsic properties. On the other hand, MSHA accounts for halo-exclusion (see e.g., Porciani & Giavalisco 2002; Balaguera-Antolínez 2014; García & Rozo 2019) by implementing a so-called multi-scale algorithm (MS hereafter) described by Balaguera-Antolínez et al. (2023).

The main idea behind the MS approach is that tracers with largest values of primary properties η_p (e.g. virial mass, maximum circular velocity or velocity dispersion) are those delineating the statistical properties on large-scales. Accordingly, high values of such properties should be prevented from being assigned to close pairs. To achieve this, MSHA divides the range of available values of the reference primary property η_p in a number of intervals or levels. Each level is in turn characterised by a spatial mesh covering the simulation volume, whose resolution is given by the number of reference tracers with values η_p in that level, such that on average, each spatial cell within each level is populated by one tracer⁵. The exclusion effect, being linked to the size of dark matter halos, can be more pronounced towards low redshift, with the increment in the abundance of high-mass halos (see e.g. Balaguera-Antolínez 2014).

The assignment of halo properties is performed in a hierarchical order, in which a main property is assigned first (in our case, V_{\max}) and subsequent assignment campaigns follow using the information of the properties already assigned (see e.g., Sinigaglia et al. 2021, for applications to hydro-simulations). The first assignment is done explicitly using the MS technique, reading the values of the main property from the reference catalog, and assigning these to

⁵ The algorithm uses as input parameter the number of levels and the size of the mesh of each level, from which the range of the intervals in the property η_p are computed. That is, the number of tracers in each interval equals the size of the mesh given as input parameter.

mock tracers in a top-bottom order: that is, starting from the highest level (containing the highest values of η_p), it sorts the values of the properties η_p and assigns them from highest values in each level, simultaneously preventing from assigning two consecutive values of η_p to tracers living in the same spatial cell. Values below the minimum of η_p defined by the last level are assigned from the (unsorted) remaining set of reference properties, which is indeed the approach followed for all mock tracers when MS is not applied. In both cases, the process takes into account the dependencies with local and non-local properties $\{\Theta\}$ presented in §2.

The MSHA algorithm contains a number of options to prevent failed attempts to assign the main property. The main source of failure is linked to the so-called cosmic-variance, which is embodied in this scenario as the difference in the actual number of tracers in the reference and tracers in the mock in a given bin of $\{\Theta\}$. To mitigate this, the MS approach uses tolerance percentages $f_\ell \leq 1$ to reduce the number of tracers to be assigned in a given level, assigning the remaining fraction as in a non-MS scenario. In that case, if the number of requested properties is larger than the number of available properties in the reference (in a given bin of $\{\Theta\}$), the property is assigned following the conditional probability distribution $\mathcal{P}_\ell(\eta_p | \{\Theta\})$ assessed for every level ℓ . Finally, if the set of properties $\{\Theta\}_{\text{mock}}$ find no representation in the set $\{\Theta\}_{\text{ref}}$, the value of η_p assigned to the tracers is drawn from the global distribution.

The flow-chart of Fig. 1 depicts the main steps followed in the assignment of halo properties. This procedure can be generalized to any number of reference simulations (strictly speaking, an ensemble of independent realizations built from the same initial power spectrum) from which the conditional probability distributions $\mathcal{P}(\eta_p | \{\Theta\})$ can be obtained (as shown by Balaguera-Antolínez et al. 2023).

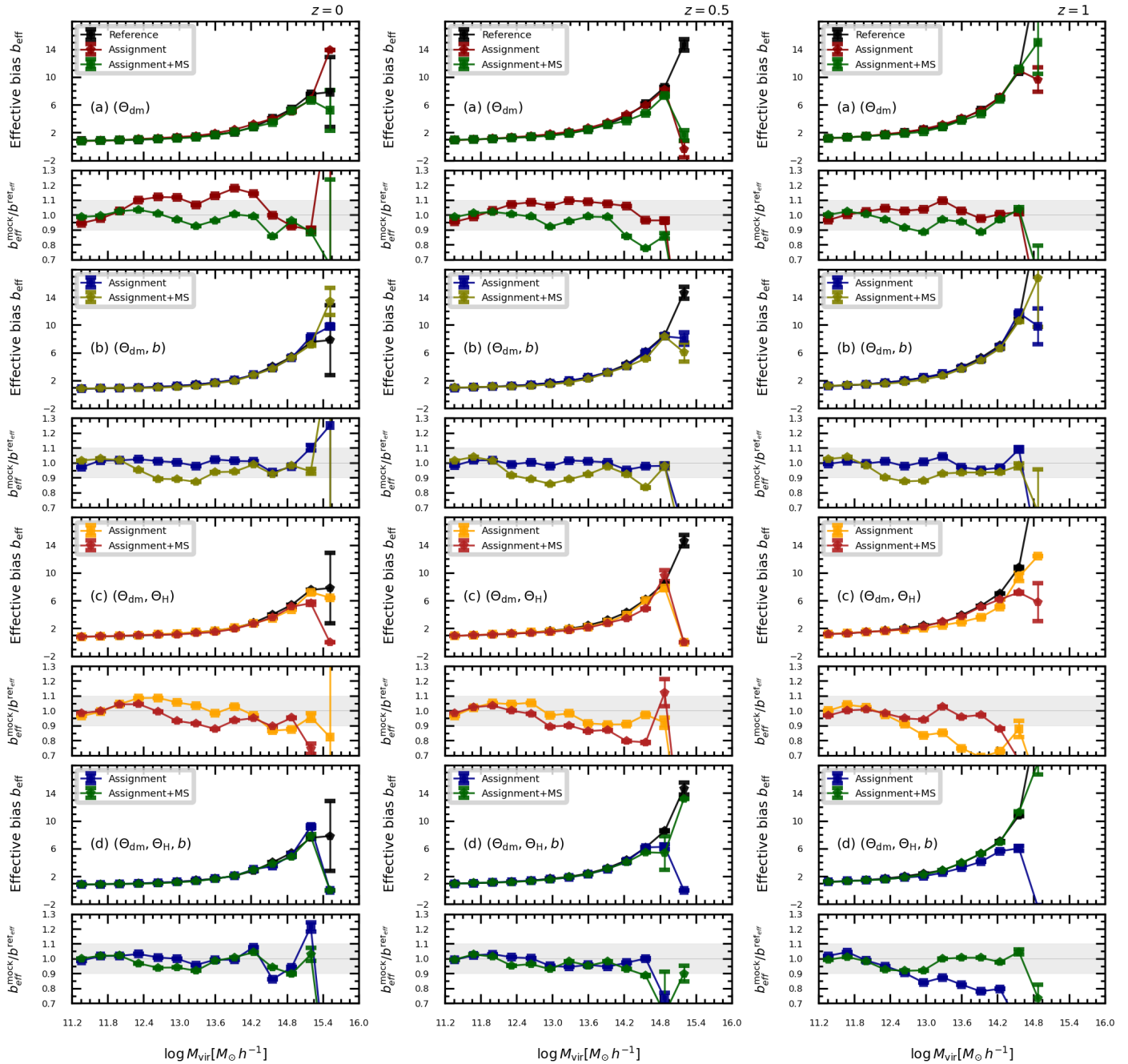


Fig. 2: Large-scale effective bias as a function of virial mass, assigned as described in §3. The main panels (a,b,c,d) show the effective bias measured from the reference and the results from the property assignment at $z=0$ (left) and $z=0.5$ (center) and $z=1$ (right column), with (labeled Assignment+MS) and without (labeled Assignment) the multi-scale approach. Panel (a) shows the results of using only dark matter properties Θ_{dm} in the assignment of maximum circular velocity and virial mass. Panel (b) shows the results of adding the information from the individual bias. Panel (c) shows the results after including halo environmental properties Θ_{H} , and panel (d) shows the result of including both bias and environmental properties. The bottom panels show, in each case, the ratio to the primary bias obtained from the mock catalog using its original properties (the latter shown as black points in all main panels). The gray region in these bottom panels depicts 10% deviation with respect to unity. The error bars denote the error on the mean bias-property relation.

4. Application

We use a set of paired and fixed-amplitude N -body simulations (at redshift $z=0, 0.5$ and $z=1$) to show the performance of the method. This represents the set reference-mock. With this type of simulations, even if the initial conditions display the same amplitude of power spectrum, dif-

ferences in the occupancy of the bins designed to build the scaling relations can arise through gravitational evolution-coupling of initially randomly distributed phases (see e.g., Angulo & Pontzen 2016; Villaescusa-Navarro et al. 2018).

Following the procedure described in §3, we assign maximum circular velocities to the halos in the mock simula-

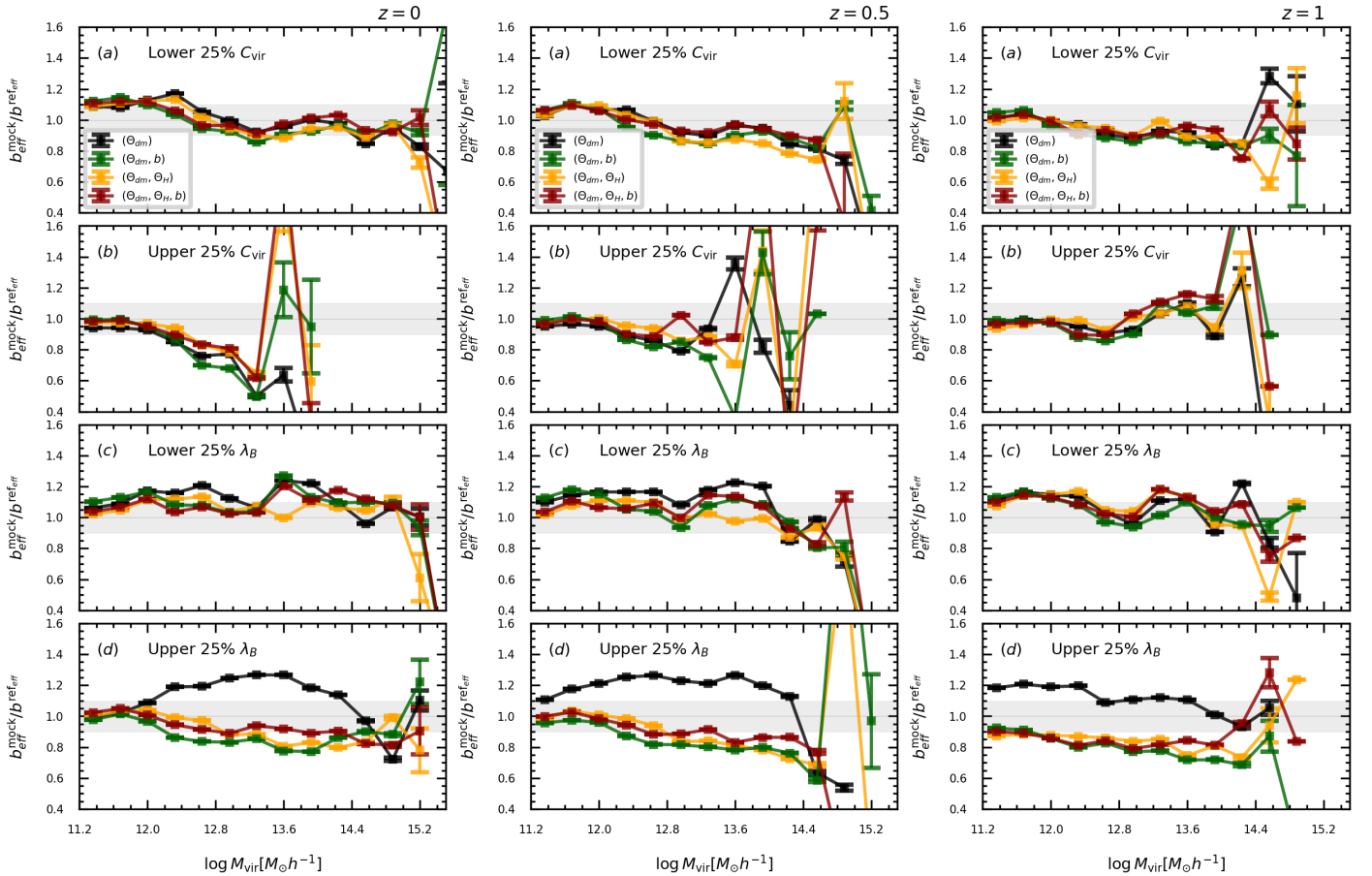


Fig. 3: Secondary effective bias as a function of halo virial mass. This plot compares (with ratios) the effective bias measured reference and the mock after assignment, at two different cosmological redshifts (shown in different columns) and using different combinations of halo/dark matter properties, as shown in the legends. Panels (a) and (b) show the secondary bias using halo concentration, for the lower and upper quartiles computed in each mass bin, respectively. Similarly, panels (c) and (d) shows secondary bias as a function of halo spin. In all plots the shaded region denotes a 10% deviation from unity. In all cases, MS is employed. The error bars are computed from adding in quadrature the corresponding uncertainties in each bias estimate.

tion on top of which we assign virial mass⁶ through the assessment of the probability distribution $\mathcal{P}(M_{\text{vir}}^{\text{ref}} | V_{\text{max}}^{\text{ref}}, \{\Theta\}_{\text{ref}})$, sampling as:

$$M_{\text{vir}} \sim \mathcal{P}(M_{\text{vir}}^{\text{ref}} | V_{\text{max}}^i \in \Delta V_{\text{max}}^{\text{ref}}, \{\Theta\}_{\text{ref}} = \{\Theta\}_{\text{mock}}). \quad (2)$$

⁶ For the assignment of V_{max} using MS, we have used three levels with sizes $16^3, 64^3, 128^3$, with 100 bins in local density, 4 cosmic-web types, 10 bins in local overdensity, 10 bins in Mach number and 15 bins in large-scale bias. The tolerance factors are chosen to be 0.9 for all levels. At $z=0$, the fraction of V_{max} assigned in each level is $\sim 0.01, 1.2$ and $\sim 10\%$ of the total number of available tracers, for levels $\ell=1$ (most massive halos), $\ell=2$ and $\ell=3$ respectively. Below the last level, no MS is applied; in this case, $\sim 70\%$ of tracers are assigned a property from the reference, while the remaining fraction are assigned a property using the global distribution. For the assignment of virial mass and secondary properties, 100 bins in V_{max} and M_{vir} are used, respectively. This set-up leads to $\sim 3, 7, 8$ and 12% global differences in abundance with respect to the reference, when measured as a function of $V_{\text{max}}, M_{\text{vir}}, C_{\text{vir}}$ and λ_B respectively.

In Fig.2 we present the impact of the property assignment in the large-scale effective bias as a function of virial mass⁷. In particular, we show three different scenarios, namely i) assignment using only dark matter properties, ii) adding the effective bias, iii) using dark matter and halo environmental properties and iv) adding the effective bias the previous set, for three cosmological redshifts ($z=0, 0.5, 1$). In each of these cases, we present the results with and without the MS approach applied in the assignment of V_{max} .

In general, Fig. 2 shows that the implementation of the information of halo environmental properties and the large-scale bias yields a clustering signal in agreement, on large scales, with the clustering signal measured from the mock catalog using the original properties, especially on the high mass halo population (where the impact of the MS approach is noticeable, given that exclusion effects are more dominant as long as $z \rightarrow 0$ and at large scales). It also is observed that as long as we approach $z=0$, the presence for properties beyond those of the dark matter is more evident (we have

⁷ Even if the first assignment corresponds to V_{max} , we show the results in terms of M_{vir} as it is more familiar within the large-scale structure community

verified this trend performing the same analysis at $z = 0.5$ and $z = 3$).

We now use halo concentration C_{vir} and halo dimensionless spin λ_B as example of the assignment of secondary properties. To establish the hierarchical approach to the assignment of properties, we refer to Balaguera-Antolínez et al. (2024), where it was shown that the correlation between halo concentration and mass is larger than that between mass and halo spin. Accordingly, we start by assigning halo concentration by measuring from the reference the scaling relation $\mathcal{P}(C_{\text{vir}}|M_{\text{vir}}^{\text{ref}}, \{\Theta\}_{\text{ref}})$ and sampling from it as

$$C_{\text{vir}} \curvearrowright \mathcal{P}(C_{\text{vir}}^{\text{ref}} | M_{\text{vir}}^i \in \Delta M_{\text{vir}}^{\text{ref}}, \{\Theta\}_{\text{ref}} = \{\Theta\}_{\text{mock}}), \quad (3)$$

where the masses M_{vir}^i correspond to the values assigned with Eq. (2). Similarly, for the assignment of halo spin, we measure the scaling relation $\mathcal{P}(\lambda_B|M_{\text{vir}}^{\text{ref}}, C_{\text{vir}}^{\text{ref}}, \{\Theta\}_{\text{H,ref}}, \{\Theta_H\})$ and sample values as

$$\lambda_B \curvearrowright \mathcal{P}(\lambda_B^{\text{ref}} | M_{\text{vir}}^i \in \Delta M_{\text{vir}}^{\text{ref}}, C_{\text{vir}}^i \in \Delta C_{\text{vir}}^{\text{ref}}, \Theta_{\text{ref,H}} = \Theta_{\text{mock,H}}), \quad (4)$$

where we have not included the dark matter properties, and solely relied on the halo intrinsic and environmental properties.

To assess the precision of the the signal of secondary bias, we divide the sample in quartiles of the secondary property and measure the mean effective bias in bins of a primary property. In Fig. 3 we display the ratios of effective bias in these two quartiles of the secondary properties with respect to the same signal measured from the reference simulations, and for three different snapshots of the UNITSim. In general, all tests display $\sim 10\%$ discrepancy with respect to the reference. The largest difference is obtained when only dark matter properties are used, in agreement with previous results in the literature. The inclusion of halo environmental properties Θ_H and/or effective bias contribute to assign halo properties with a secondary bias signature within $\sim 10\%$ difference with respect to the reference. The results of Fig. 3 have been obtained using MS, and we have verified that such choice produce better results than the case without MS at the redshifts **shown in that figure**.

5. Discussion

Our results show that the use of individual effective bias (Eq. 1) can be relevant in the process of reconstructing and/or assigning halo properties to generate reliable halo mock catalogs that follow the expected large-scale clustering signal. While the absence of the information on effective bias or environmental halo properties in the assignment can still generate robust scaling relations between halo properties (specially towards high redshifts, as seen in panels (a) of Fig.2), their use can improve the resulting clustering signal. The signal of mean large-scale primary bias (i.e., as shown in Fig. 2) is one of the key probes in the clustering analysis of current galaxy redshift surveys (see e.g., Tutusaus et al. 2020), as it can provide insights on the galaxy/cluster scaling relations (see e.g., Cooray & Sheth 2002; Balaguera-Antolínez 2014; Shi & Sheth 2018) and physics of the early Universe (i.e., primordial non-Gaussianities, see e.g., Gianantonio et al. 2012; Euclid Collaboration et al. 2023b). As such, it is important to minimize deviations in the mean primary bias (with respect to the results of N -body simulations) when constructing mock catalogs, as it can propagate

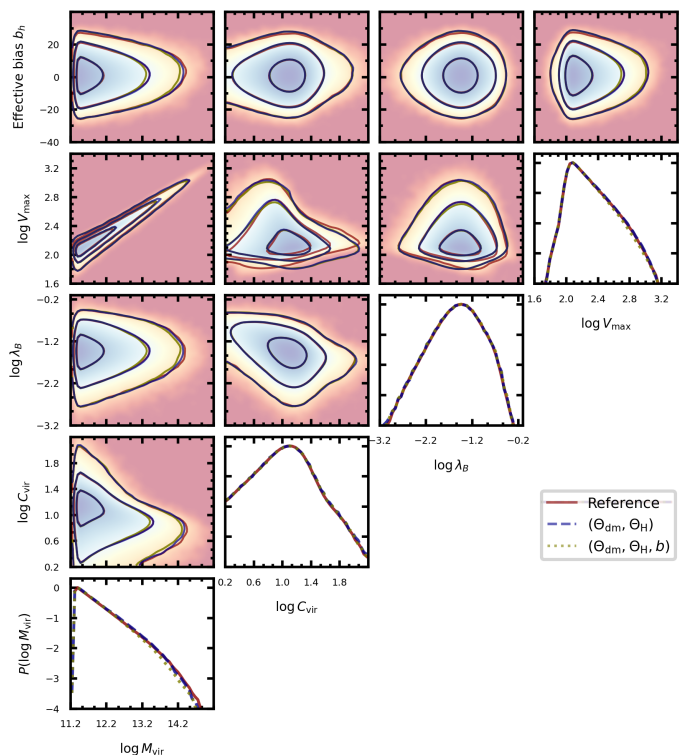


Fig. 4: 2D scaling relations between halo properties and large-scale halo effective bias in the UNITSim at $z = 0$. The different lines in the contours (denoting surfaces of equal number of tracers) and the 1D distributions show the result from different set-ups in the assignment algorithm, as shown in the legend.

from the covariance matrix to the likelihood and lead to biased results (Artis et al. 2021; Euclid Collaboration et al. 2023a)

The inclusion of environmental halo properties and effective bias is also key (to a evident degree though) if secondary bias (key for assessing the impact of e.g., HOD assumptions on the galaxy population, see e.g., Hearin et al. (2016); Lehmann et al. (2017)) is expected to be present in the mock catalog. It can be shown that effective bias as a function of, e.g., virial mass, in quartiles $\Delta\eta_s = \Delta\eta_s(M_{\text{vir}})$ of a secondary property η_s can be mathematically decomposed as

$$\langle b|M_{\text{vir}} \rangle_{\Delta\eta_s} = \int d\tilde{M}_{\text{vir}} \langle b|\tilde{M}_{\text{vir}} \rangle F_{\Delta\eta_s}(M_{\text{vir}}, \tilde{M}_{\text{vir}}), \quad (5)$$

where $\langle b|\tilde{M}_{\text{vir}} \rangle$ is the primary bias,

$$F_{\Delta\eta_s}(M_{\text{vir}}, \tilde{M}_{\text{vir}}) \equiv \int_{\Delta\eta_s} d\eta_s \mathcal{P}(\eta_s|M_{\text{vir}}) \mathcal{P}(\tilde{M}_{\text{vir}}|\eta_s), \quad (6)$$

and $\mathcal{P}(\eta_s|M_{\text{vir}})$ denotes the scaling relation between η_p and M_{vir} . Thus, the signal of secondary bias (e.g., as shown in Fig. 3) is sensitive to the full scaling relation (i.e., all the moments of the conditional probability distribution $\mathcal{P}(\eta_s|M_{\text{vir}})$). In Fig. 4 we show the 2D and 1D distribution of halo properties and effective bias from the reference simulation as well as from the different experiments performed in this paper. While there are sizable differences (for example, in the $V_{\text{max}} - C_{\text{vir}}$ relation), in general, the reconstruction of the halo properties provides not only a robust set of halo-scaling relations, but also reconstructs the large-scale halo

connection through primary ($\leq 5\%$) and secondary ($\leq 15\%$ differences) bias, as can be read from Figs. 3 and 4.

The performance of the MSHA algorithm can depend on how detailed the different scaling relations (assessed from the reference and to be sampled onto the mock catalog) are determined. However, the level of refinement is not arbitrary as we can eventually enter an overfitting regime. This can eventually precipitate a failed attempt to assign properties when a new set of density field (or another realization of the reference fields) and its halo distribution is used as a target mock and, as such, a limit in the number of bins (or tolerance thresholds) is imposed.

In Fig. 5 we present an example of the scaling relation between the assigned halo mass and the true value of that property as read from the reference simulation used as mock catalog (at $z = 0$). In general, there is a large scatter between the true and assigned property, which varies little among the different set-ups shown. In Fig. 6 we display the correlation coefficient between the properties shown in Fig. 5 for halos with true and assigned masses above the values in the x-axis, indicating that in general the reconstruction improves towards large halo masses. The large scatter seen at the low halo mass region likely arises from the degeneracies between the different dark matter properties (e.g. cosmic-web types) and the mass of the halos hosted therein, which cannot be broken by the inclusion of large scale bias (as it also shows large scatter with respect to halo mass, see e.g., Balaguera-Antolínez et al. 2024). While the impact of such degeneracy is small when measuring the signal of large-scale effective bias, it can be crucial when populating intermediate and low mass halos with galaxies. In forthcoming work we will add learning algorithms to reduce this scatter and provide a more accurate reconstruction of halo properties.

6. Conclusions

In this paper we have described a strategy to assign intrinsic halo properties in halo mock catalogs generated with the so-called calibrated methods (see e.g., Balaguera-Antolínez et al. 2019). These methods can provide sets of independent halo realizations with phase-space coordinates and their underlying dark matter density field, lacking though of intrinsic halo properties, which are key in order to generate galaxy mock catalogs using, for example, an HOD approach (see e.g., Monaco et al. 2013; Alam et al. 2020; Euclid Collaboration et al. 2024).

While the assignment of halo properties can be accurately performed based on the abundance or conditional probability distributions, the resulting two-point statistics on large-scales, expressed as a function of that particular property, is not fully captured (see for example Zhao et al. 2015; Balaguera-Antolínez et al. 2023). A higher precision in the clustering signal (with respect to N -body estimates) can be achieved when conditional mass (or any other property) function are implemented, using local (i.e. density) and non-local (i.e. tidal field) information of the underlying dark matter density field. Nevertheless, such ingredients cannot induce the correct signal of large-scale effective bias, specially for massive tracers.

With the possibility of individually computing large-scale bias for dark matter tracers (see e.g., Paranjape et al. 2018; Contreras et al. 2021; Balaguera-Antolínez et al.

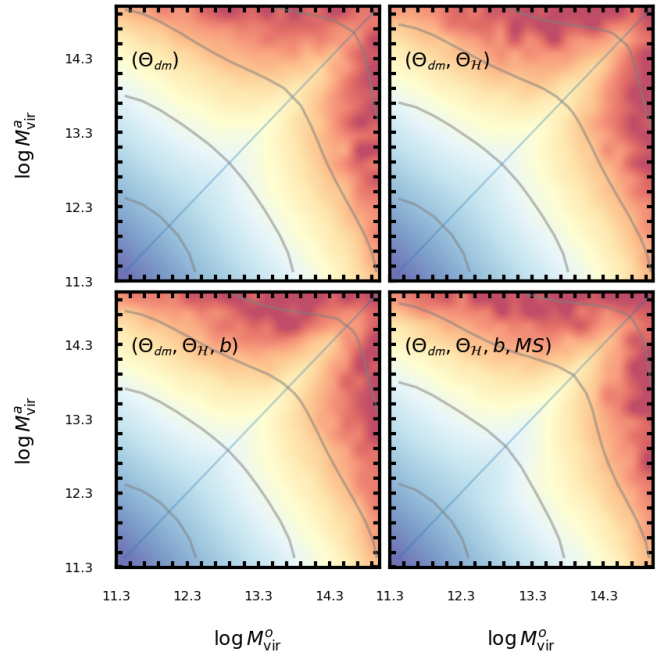


Fig. 5: Scaling relation between the logarithm of the assigned virial mass M_{vir}^a and the logarithm of the true virial mass M_{vir}^o , for four different set-ups in the assignment algorithm (at $z = 0$). The color coding and contours indicate constant number of tracers from high (blue) to low (red).

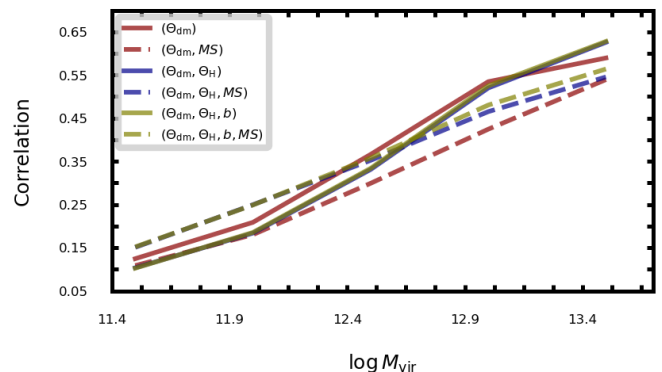


Fig. 6: Correlation coefficient between the assigned mass and the original mass at $z = 0$ for different set-ups used in the assignment algorithm, for cuts in the true and assigned masses $M_{\text{vir}}^a, M_{\text{vir}}^o > M_{\text{vir}}$

2024), it is feasible to assign intrinsic halo properties ensuring that the two-point statistics, in particular, the signal of primary and secondary halo bias measured on large-scales is closer to what is measured from a, e.g., N -body simulation. The algorithm described in this paper makes use of this fact, complementing it with with a so-called multi-scaling approach, designed to account for the phenomena of halo exclusion. It can implement other dark matter properties, such as tidal anisotropy, peak statistics (see e.g., Peacock & Heavens 1985) or the shear velocity field (see e.g., Libeskind et al. 2018). Similarly, other non-local halo properties such as the neighbor statistics can be included.

We can summarize the main results of this paper as follows:

- Using the information of the halo individual large-scale bias, environmental halo and dark matter properties plus the multi-scale approach, the MSHA algorithm can assign intrinsic properties to dark matter halos with a resulting large-scale primary bias (i.e., expressed as a function of primary properties such as virial mass or maximum circular velocity) within $\sim 5\%$ precision with respect to the signal obtained using the properties in the the reference simulation (see Fig. 2).
- The reconstruction of the secondary bias is also favored by the inclusion of the large-scale individual bias, although the differences among the different set-ups shown in Fig. 3 are rather small.
- As a byproduct of the reconstruction of halo bias, halo properties, such as virial mas, are also recovered. This yields correlations between assigned and original halo properties of ~ 0.5 for high masses, as shown in Fig. 5. We note that the algorithm in its current state is not specifically designed to recover halo properties with high precision, but to replicate the property-bias relation.
- Our results motivate further developments of this algorithm, using, e.g., learning techniques, that helps to improve the precision in the reconstruction of intrinsic properties, especially for low mass halos, which is key to the assignment of galaxies to dark matter halos in mock catalogs generated with approximated methods.

Acknowledgements. We would like to thank the referee for her/his review, which helped in the presentation of our results. We would like to thank J.Garcia-Farieta for comments on the manuscript. We also acknowledge Chia-Hsun Chuang, Gustavo Yépez and F.-S. Kitaura for granting access to the UNITSim. ABA acknowledges the Spanish Ministry of Economy and Competitiveness (MINECO) under the Severo Ochoa program SEV-2015-0548 grants. The UNITSim has been run at the MareNostrum Supercomputer hosted by the Barcelona Supercomputing Center, Spain, with computing time granted by PRICE under grant number 2016163937. ADMMD thanks the IAC facilities and Fondecyt for financial support through the Fondecyt Regular 2021 grant 1210612. No AI application has been used to generate neither text, figures data, nor code for this article.

References

Agarwal, S. & Feldman, H. A. 2013, MNRAS, 432, 307
 Alam, S., Peacock, J. A., Kraljic, K., Ross, A. J., & Comparat, J. 2020, MNRAS, 497, 581
 Amendola, L., Appleby, S., Avgoustidis, A., et al. 2016, ArXiv e-prints, arXiv:1606.00180
 Angulo, R. E., Baugh, C. M., & Lacey, C. G. 2008, MNRAS, 387, 921
 Angulo, R. E. & Hahn, O. 2022, Living Reviews in Computational Astrophysics, 8, 1
 Angulo, R. E. & Pontzen, A. 2016, MNRAS, 462, L1
 Aragon-Calvo, M. A. 2016, MNRAS, 455, 438
 Artis, E., Melin, J.-B., Bartlett, J. G., & Murray, C. 2021, A&A, 649, A47
 Avila, S., Murray, S. G., Knebe, A., et al. 2015, MNRAS, 450, 1856
 Balaguera-Antolínez, A. 2014, A&A, 563, A141
 Balaguera-Antolínez, A., Kitaura, F.-S., Alam, S., et al. 2023, A&A, 673, A130
 Balaguera-Antolínez, A., Kitaura, F.-S., Pellejero-Ibáñez, M., et al. 2020, MNRAS, 491, 2565
 Balaguera-Antolínez, A., Kitaura, F.-S., Pellejero-Ibáñez, M., Zhao, C., & Abel, T. 2019, MNRAS, 483, L58
 Balaguera-Antolínez, A., Montero-Dorta, A. D., & Favole, G. 2024, A&A, 685, A61
 Balaguera-Antolínez, A., Sánchez, A. G., Böhringer, H., & Collins, C. 2012, MNRAS, 425, 2244

Baratta, P., Bel, J., Gouyou Beauchamps, S., & Carbone, C. 2022, arXiv e-prints, arXiv:2211.13590
 Baratta, P., Bel, J., Plaszczynski, S., & Ealet, A. 2020, A&A, 633, A26
 Bartlett, D. J., Ho, M., & Wandelt, B. D. 2024, arXiv e-prints, arXiv:2405.00635
 Behroozi, P. S., Wechsler, R. H., & Wu, H.-Y. 2013, ApJ, 762, 109
 Benitez, N., Dupke, R., Moles, M., et al. 2014, arXiv e-prints, arXiv:1403.5237
 Berlind, A. A. & Weinberg, D. H. 2002, ApJ, 575, 587
 Berner, P., Refregier, A., Sgier, R., et al. 2022, J. Cosmology Astropart. Phys., 2022, 002
 Bond, J. R. & Myers, S. T. 1996, ApJS, 103, 1
 Bullock, J. S., Dekel, A., Kolatt, T. S., et al. 2001, ApJ, 555, 240
 Chuang, C.-H., Yepes, G., Kitaura, F.-S., et al. 2019, MNRAS, 487, 48
 Conroy, C., Wechsler, R. H., & Kravtsov, A. V. 2006, ApJ, 647, 201
 Contreras, S., Angulo, R. E., & Zennaro, M. 2021, MNRAS, 504, 5205
 Contreras, S., Zehavi, I., Padilla, N., et al. 2019, MNRAS, 484, 1133
 Cooray, A. 2002, ApJ, 576, L105
 Cooray, A. & Sheth, R. 2002, Phys. Rep., 372, 1
 Croton, D. J., Gao, L., & White, S. D. M. 2007, MNRAS, 374, 1303
 Dalal, N., White, M., Bond, J. R., & Shirokov, A. 2008, ApJ, 687, 12
 de Santi, N. S. M., Rodrigues, N. V. N., Montero-Dorta, A. D., et al. 2022, MNRAS, 514, 2463
 Ding, S., Lavaux, G., & Jasche, J. 2024, arXiv e-prints, arXiv:2407.01391
 Dubois, Y., Beckmann, R., Bournaud, F., et al. 2021, A&A, 651, A109
 Euclid Collaboration, Castander, F. J., Fosalba, P., et al. 2024, arXiv e-prints, arXiv:2405.13495
 Euclid Collaboration, Castro, T., Fumagalli, A., et al. 2023a, A&A, 671, A100
 Euclid Collaboration, Sciotti, D., Gouyou Beauchamps, S., et al. 2023b, arXiv e-prints, arXiv:2310.15731
 Faltenbacher, A. & White, S. D. M. 2010, ApJ, 708, 469
 Fang, F., Cai, Y.-C., Li, Z., et al. 2024, MNRAS, 530, 2355
 Favole, G., Comparat, J., Prada, F., et al. 2016, MNRAS, 461, 3421
 Feldmann, R., Quataert, E., Faucher-Giguère, C.-A., et al. 2023, MNRAS, 522, 3831
 Feng, Y., Chu, M.-Y., Seljak, U., & McDonald, P. 2016, MNRAS, 463, 2273
 Forero-Romero, J. E., Hoffman, Y., Gottlöber, S., Klypin, A., & Yepes, G. 2009, MNRAS, 396, 1815
 Forero-Sánchez, D., Chuang, C.-H., Rodriguez-Torres, S., et al. 2022, Monthly Notices of the Royal Astronomical Society, 513
 Fry, J. N. & Gaztanaga, E. 1993, ApJ, 413, 447
 Gao, L., Springel, V., & White, S. D. M. 2005, MNRAS, 363, L66
 Gao, L. & White, S. D. M. 2007, MNRAS, 377, L5
 García, R. & Rozo, E. 2019, MNRAS, 489, 4170
 Garrison, L. H., Eisenstein, D. J., Ferrer, D., et al. 2018, ApJS, 236, 43
 Giannantonio, T., Porciani, C., Carron, J., Amara, A., & Pillepich, A. 2012, MNRAS, 422, 2854
 Hahn, O., Porciani, C., Carollo, C. M., & Dekel, A. 2007, MNRAS, 375, 489
 Han, J., Li, Y., Jing, Y., et al. 2019, MNRAS, 482, 1900
 He, S., Li, Y., Feng, Y., et al. 2019, Proceedings of the National Academy of Science, 116, 13825
 Hearin, A. P., Zentner, A. R., van den Bosch, F. C., Campbell, D., & Tollerud, E. 2016, MNRAS, 460, 2552
 Howlett, C., Manera, M., & Percival, W. J. 2015, Astronomy and Computing, 12, 109
 Izard, A., Fosalba, P., & Crocce, M. 2018, MNRAS, 473, 3051
 Kaiser, N. 1984, ApJ, 284, L9
 Kauffmann, G., Nusser, A., & Steinmetz, M. 1997, MNRAS, 286, 795
 Kitaura, F.-S., Balaguera-Antolínez, A., Sinigaglia, F., & Pellejero-Ibáñez, M. 2022, Monthly Notices of the Royal Astronomical Society, 512, 2245
 Kitaura, F.-S., Yepes, G., & Prada, F. 2014, MNRAS, 439, L21
 Klypin, A., Prada, F., & Byun, J. 2020, MNRAS, 496, 3862
 Knebe, A., Knollmann, S. R., Muldrew, S. I., et al. 2011, MNRAS, 415, 2293
 Koda, J., Blake, C., Beutler, F., Kazin, E., & Marin, F. 2016, MNRAS, 459, 2118
 Kravtsov, A. V., Berlind, A. A., Wechsler, R. H., et al. 2004, ApJ, 609, 35
 Lazeyras, T., Musso, M., & Schmidt, F. 2017, Journal of Cosmology and Astro-Particle Physics, 2017, 059
 Lee, C. T., Primack, J. R., Behroozi, P., et al. 2017, MNRAS, 4, 3834
 Lee, J. & Moon, J.-S. 2024, arXiv e-prints, arXiv:2406.11182

- Lehmann, B. V., Mao, Y.-Y., Becker, M. R., Skillman, S. W., & Wechsler, R. H. 2017, *ApJ*, 834, 37
- Levi, M., Bebek, C., Beers, T., et al. 2013, *ArXiv e-prints*, arXiv:1308.0847
- Libeskind, N. I., van de Weygaert, R., Cautun, M., et al. 2018, *MNRAS*, 473, 1195
- Maksimova, N. A., Garrison, L. H., Eisenstein, D. J., et al. 2021, *MNRAS*, 508, 4017
- Manera, M., Scoccimarro, R., Percival, W. J., et al. 2013, *MNRAS*, 428, 1036
- Mansfield, P. & Avestruz, C. 2021, *MNRAS*, 500, 3309
- Mansfield, P. & Kravtsov, A. V. 2020, *MNRAS*, 493, 4763
- Mao, Y.-Y., Zentner, A. R., & Wechsler, R. H. 2018, *MNRAS*, 474, 5143
- Meriot, R., Khochfar, S., Oñorbe, J., & Smith, B. 2022, *MNRAS*, 512, 27
- Mo, H., van den Bosch, F. C., & White, S. 2010, *Galaxy Formation and Evolution*
- Monaco, P., Sefusatti, E., Borgani, S., et al. 2013, *MNRAS*, 433, 2389
- Monaco, P., Theuns, T., & Taffoni, G. 2002, *MNRAS*, 331, 587
- Montero-Dorta, A. D., Artale, M. C., Abramo, L. R., et al. 2020, *MNRAS*, 496, 1182
- Montero-Dorta, A. D., Chaves-Montero, J., Artale, M. C., & Favole, G. 2021, *MNRAS*, 508, 940
- Montero-Dorta, A. D., Pérez, E., Prada, F., et al. 2017, *ApJ*, 848, L2
- Montero-Dorta, A. D. & Rodríguez, F. 2024, *MNRAS*, 531, 290
- Munari, E., Monaco, P., Koda, J., et al. 2017, *Journal of Cosmology and Astro-Particle Physics*, 2017, 050
- Musso, M., Cadiou, C., Pichon, C., et al. 2018, *MNRAS*, 476, 4877
- Nagamine, K., Ostriker, J. P., & Cen, R. 2001, *ApJ*, 553, 513
- Navarro, J. F., Frenk, C. S., & White, S. D. M. 1996, *ApJ*, 462, 563
- Nelson, D., Springel, V., Pillepich, A., et al. 2019, *Computational Astrophysics and Cosmology*, 6, 2
- Paranjape, A. & Alam, S. 2020, *MNRAS*, 495, 3233
- Paranjape, A., Hahn, O., & Sheth, R. K. 2018, *MNRAS*, 476, 3631
- Peacock, J. A. & Heavens, A. F. 1985, *Monthly Notices of the Royal Astronomical Society*, 217, 805
- Pellejero-Ibañez, M., Balaguera-Antolínez, A., Kitaura, F.-S., et al. 2020, *MNRAS*, 493, 586
- Piras, D., Joachimi, B., & Villaescusa-Navarro, F. 2023, *MNRAS*, 520, 668
- Pollack, J. E., Smith, R. E., & Porciani, C. 2014, *MNRAS*, 440, 555
- Porciani, C. & Gialvalisco, M. 2002, *ApJ*, 565, 24
- Ramakrishnan, S., Paranjape, A., Hahn, O., & Sheth, R. K. 2019, *MNRAS*, 489, 2977
- Ramakrishnan, S., Paranjape, A., & Sheth, R. K. 2021, *MNRAS*, 503, 2053
- Rodrigues, N. V. N., de Santi, N. S. M., Montero-Dorta, A. D., & Abramo, L. R. 2023, *MNRAS*, 522, 3236
- Sato-Polito, G., Montero-Dorta, A. D., Abramo, L. R., Prada, F., & Klypin, A. 2019, *MNRAS*, 487, 1570
- Schaye, J., Kugel, R., Schaller, M., et al. 2023, *MNRAS*, 526, 4978
- Scoccimarro, R. & Sheth, R. K. 2002, *MNRAS*, 329, 629
- Sheth, R. K. & Tormen, G. 2004, *Monthly Notices of the Royal Astronomical Society*, 350, 1385
- Shi, J. & Sheth, R. K. 2018, *MNRAS*, 473, 2486
- Sinigaglia, F., Kitaura, F.-S., Balaguera-Antolínez, A., et al. 2021, *ApJ*, 921, 66
- Skibba, R. A. & Macciò, A. V. 2011, *MNRAS*, 416, 2388
- Smith, R. E., Hernández-Monteagudo, C., & Seljak, U. 2009, *Phys. Rev. D*, 80, 063528
- Sousbie, T., Courtois, H., Bryan, G., & Devriendt, J. 2008, *ApJ*, 678, 569
- Spergel, D., Gehrels, N., Baltay, C., et al. 2015, *arXiv e-prints*, arXiv:1503.03757
- Tassev, S., Zaldarriaga, M., & Eisenstein, D. J. 2013, *J. Cosmology Astropart. Phys.*, 6, 036
- Tinker, J. L., Robertson, B. E., Kravtsov, A. V., et al. 2010, *ApJ*, 724, 878
- Tutusaus, I., Martinelli, M., Cardone, V. F., et al. 2020, *A&A*, 643, A70
- Vale, A. & Ostriker, J. P. 2004, *MNRAS*, 353, 189
- van de Weygaert, R., Aragon-Calvo, M. A., Jones, B. J. T., & Platen, E. 2009, *ArXiv e-prints*, arXiv:0912.3448
- Villaescusa-Navarro, F., Anglés-Alcázar, D., Genel, S., et al. 2021, *ApJ*, 915, 71
- Villaescusa-Navarro, F., Naess, S., Genel, S., et al. 2018, *ApJ*, 867, 137
- Wechsler, R. H., Zentner, A. R., Bullock, J. S., Kravtsov, A. V., & Allgood, B. 2006, *ApJ*, 652, 71
- White, M., Tinker, J. L., & McBride, C. K. 2014, *MNRAS*, 437, 2594
- Wong, A. W. C. & Taylor, J. E. 2012, *ApJ*, 757, 102
- Wu, J. F., Kragh Jespersen, C., & Wechsler, R. H. 2024, *arXiv e-prints*, arXiv:2402.07995
- Xu, X., Zehavi, I., & Contreras, S. 2021, *MNRAS*, 502, 3242
- Yang, X., Zhang, Y., Lu, T., et al. 2017, *ApJ*, 848, 60
- Zehavi, I., Kerby, S. E., Contreras, S., et al. 2019, *ApJ*, 887, 17
- Zhai, Z., Benson, A., Wang, Y., Yepes, G., & Chuang, C.-H. 2019, *MNRAS*, 490, 3667
- Zhang, X., Wang, Y., Zhang, W., et al. 2019, *arXiv e-prints*, arXiv:1902.05965
- Zhao, C., Kitaura, F.-S., Chuang, C.-H., et al. 2015, *MNRAS*, 451, 4266
- Zhou, S., Zhang, P., & Chen, Z. 2023, *MNRAS*, 523, 5789